ACS Catalysis

RESEARCH ARTICLE

pubs.acs.org/acscatalysis

Aerobic Oxidation of Hydrocarbons Catalyzed by Mn-Doped Nanoporous Aluminophosphates(I): Preactivation of the Mn Sites

Luis Gómez-Hortigüela,* Furio Corà,* and C. Richard A. Catlow

Department of Chemistry, University College London, 20 Gordon Street, WC1H 0AJ London, United Kingdom

ABSTRACT: We apply state of the art electronic structure techniques, based on hybrid exchange-functionals in DFT and periodic boundary conditions, to unravel the reaction mechanism responsible for the initial stages of the aerobic oxidation of hydrocarbons catalyzed by Mn-doped aluminophosphates. In this preactivation step of the catalyst, which precedes the catalytic propagation cycle in which the final oxidation products (alcohol, aldehyde, and carboxylic acid) are formed, the Mn^{III} ions initially present in the activated (calcined) catalyst are transformed by interaction with one alkane and one O_2 molecule into new Mn-bearing species: a reduced Mn^{II} site and a $Mn^{III}\cdots$peroxo complex, which are active for the subsequent propagation cycle. The preactivation step has a high activation energy, calculated as 135 kJ/mol, explaining the long induction time observed experimentally. Our results further show that Mn^{III} sites are able to produce the hydroperoxide intermediate from the reactants; however, this intermediate can be transformed into the oxidative products only through reduced Mn^{II} sites. The latter are formed from Mn^{III} in the preactivation step, via a H-abstraction from the hydrocarbon, also yielding an alkyl radical (R•) that subsequently adds O_2 in a stereospecific way to form a free peroxo radical, ROO•. Migration of ROO• in the AlPO nanopores frees Mn^{II} for the propagation cycle and forms $Mn^{III}\cdots$ROO• complexes also needed for propagation. We demonstrate the essential role of Mn^{III} active sites at the initial stages of the reaction for activating the hydrocarbon molecules; such hydrocarbon activation catalyzed by Mn requires much lower activation energies than through noncatalytic pathways, where the hydrocarbon is activated by O_2 alone.

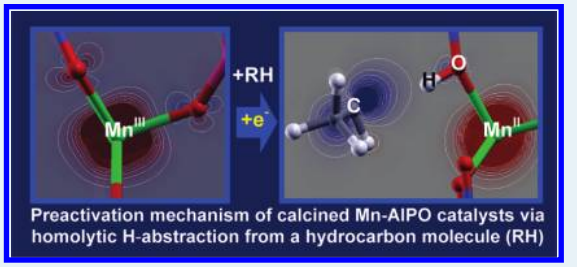

KEYWORDS: oxidation, reaction mechanism, preactivation, nanoporous aluminophosphate, hydrocarbon, zeolite, molecular modeling, heterogeneous catalysis

INTRODUCTION

Saturated hydrocarbons are among the most abundant yet inert organic compounds, and their selective oxyfunctionalization at low temperatures is a key goal in contemporary catalytic chemistry. Moreover, terminally oxidized alkanes, such as linear alcohols or acids, are of great importance as feedstocks for the chemical and pharmaceutical industries, and the need for such chemicals has prompted an intensive search for new selective oxidation reactions.

Traditionally, oxidation reactions of alkanes have been catalyzed by dissolved salts of redox-active metals; however, current environmental pressure provides a strong incentive to search for heterogeneous catalytic systems due to the well-known problems of homogeneous catalysts associated with handling and reprocessing. Molecular dioxygen is the most environmentally benign and readily available oxidant and is the oxidant of choice if suitable catalysts can be developed; however, this goal still eludes industrial-scale applications. In contrast, the natural biological cycle is supported by atmospheric oxygen, efficiently activated in a number of enzymatic reactions; man-made catalysts are still a long way from achieving the activity and selectivity that evolution has achieved in biosystems.

It is in this context that crystalline nanoporous aluminophosphate materials (AlPOs) enter the scenario: AlPOs, first discovered by Wilson et al. in 1982,[1] are zeolite-like materials in which silicon ions are replaced by phosphorus and aluminum in strict alternation, forming a 3-dimensional neutral oxide network that can adopt a range of polymorphic structures.[2] In these materials, Al and P ions can be isomorphically replaced by di-, tri-, and tetra-valent heteroatoms in a relatively easy and controllable manner, giving rise to acid, redox, and even bifunctional properties. Of particular importance for oxidation reactions are the so-called MeAPO materials in which Al ions are replaced by redox-active transition metals, such as Co, Mn, and Fe.[3−5] These materials combine the reactivity of the redox-active cations with the unique spatial constraints imposed by the molecular dimensions of their porous network.[6−9] Additional important advantages of these catalysts are their high internal surface areas, ease of preparation, and high thermal and chemical stability.[10] At present, there is extensive experimental research on their performance in a wide range of oxidation reactions, including the industrially fundamental selective oxidations of *n*-hexane[8,11,12] and cyclohexane,[13−19] the epoxidation of alkenes,[20] and the Baeyer−Villiger oxidation of ketones to lactones,[21] all using O_2 as the oxidant.

Received: October 27, 2010
Revised: November 19, 2010
Published: December 13, 2010

The exact mechanism whereby oxidation reactions are catalyzed by nanoporous MeAPOs remains unknown. There is experimental evidence that a free-radical mechanism is involved in the aerobic oxidation of hydrocarbons catalyzed by Co-, Fe-, and Mn-containing AlPOs:[8,10,16] the addition of radical initiators such as *tert*-butyl hydroperoxide dramatically reduces the otherwise observed induction period, whereas the presence of radical scavengers such as hydroquinone results in a drastic decrease of the reaction rate. In addition, the presence of a hydroperoxide derivative during the initial stages of the reaction (a compound commonly found as intermediate in free-radical oxidations) has been detected.[16] There is also evidence that the redox-active centers, and not permanently divalent sites also present in these materials, act as active sites for kinetically relevant elementary steps in alkane oxidation catalytic cycles.[9] Nevertheless, the details of the mechanism remain unclear. Such an in-depth knowledge of the reaction pathways is essential if an improvement of the regioselectivity toward the desired terminal oxyfunctionalization is to be achieved by rational design.

In free-radical autoxidations, redox-active sites homolytically decompose alkyl hydroperoxide intermediates (ROOH) via Haber−Weiss mechanisms.[22−24] The elementary steps traditionally proposed are summarized as follows:[7]

$$
\begin{aligned}
&(1) && \mathrm{RH + O_2} \rightarrow \mathrm{R\bullet + HOO\bullet}\\
&(2) && \mathrm{R\bullet + O_2} \rightarrow \mathrm{ROO\bullet}\\
&(3) && \mathrm{ROO\bullet + RH} \rightarrow \mathrm{R\bullet + ROOH}\\
&(4) && \mathrm{ROOH + Me^{II}} \rightarrow \mathrm{RO\bullet + Me^{III}OH}\\
&(5) && \mathrm{ROOH + Me^{III}OH} \rightarrow \mathrm{ROO\bullet + Me^{II} + H_2O}\\
&(6) && \mathrm{RO\bullet + RH} \rightarrow \mathrm{R\bullet + ROH}\\
&(7) && \mathrm{ROO\bullet + ROO\bullet} \rightarrow \mathrm{ROH + R(-H){=}O + O_2}
\end{aligned}
$$

The initiation reaction (1) is typically very slow, causing the induction period usually observed in these oxidations; once formed, the alkyl radicals R• rapidly add oxygen to form peroxy radicals ROO• (2), which can then propagate through H-transfer reactions to form new alkyl radicals and hydroperoxide (ROOH) (3). Reactions 2 and 3 represent a noncatalytic subcycle in which alkane and O_2 are transformed into peroxo intermediates. The latter are homolytically decomposed by the redox sites to form chain-initiating alkoxy (RO•) and alkylperoxy (ROO•) radicals (4 and 5), which undergo new propagation reactions (6 and 3). Finally, the termination step (7) involves the recombination of alkylperoxy (ROO•) radicals to form the corresponding alcohol and aldehyde in a concerted mechanism.

The aerobic oxidation of cyclohexane catalyzed by MnAPO-5, a Mn-doped aluminophosphate with the AFI framework structure, has been the subject of in-depth experimental investigations by Iglesia and co-workers,[16] employing, among others, extensive spectroscopic and isotopic labeling techniques to determine the reaction mechanism. However, the high reactivity of some of the intermediates involved makes them very difficult, if not impossible, to detect and analyze by experimental techniques. In addition, insights concerning the energetics involved (both reaction and activation energies) are needed to optimize catalyst performance, yet are difficult to obtain experimentally.

This mechanistic and energetic information can be obtained from contemporary computational electronic-structure methods, which we applied in a recent study[25] to elucidate the complete reaction mechanism of this important catalytic reaction. The reaction scheme proposed in ref 16 was employed as the starting point for our computational study; however, we also examined alternative mechanistic pathways to those proposed in ref 16, whose occurrence is difficult to characterize experimentally, but which can be effectively distinguished computationally using the calculated reaction enthalpies and activation energies.

As a prototypical reaction, we have studied the oxidation of ethane in MnAPO-5 catalysts. The choice of ethane as model hydrocarbon is due to its simple molecular structure and small volume, allowing us to use more accurate periodic DFT techniques rather than cluster models, although preventing the study of regioselectivity issues in the present work. We do, however, expect the oxidation mechanism to be largely transferable to other alkane substrates and AlPO frameworks, and so this study provides an initial point from which larger hydrocarbons and issues related to regioselectivity can be addressed in future studies.

In our previous communication, outlining the complete reaction mechanism for this reaction,[25] we showed that the main catalytic cycle requires the simultaneous presence of Mn^{II} and Mn^{III} sites, each with a particular role along the reaction: Mn^{II} is involved in the decomposition of the hydroperoxide intermediate to give the oxidative products, whereas Mn^{III} is involved in further production of hydroperoxide, for which it requires the presence of peroxo radicals. However, in the initial reaction conditions, in which the catalyst is generated by calcination of as-prepared MnAPO materials, all redox-active Mn sites are in the oxidized state (III). Furthermore, no hydroperoxide or peroxo radicals are present, and so the propagation cycle cannot take place. Therefore, a stage in which the initial components of the reaction mixture (namely, Mn^{III}, the hydrocarbon, and O_2) are transformed into species that can enter the subsequent propagation cycle, in which the main oxidative products (alcohol, aldehyde/ketone, and acid) are formed, is essential to initiate the catalytic reaction. Here, we focus on this initial stage, which we refer to as *preactivation* (I). In subsequent studies, we will report the corresponding studies concerning the *decomposition* of the hydroperoxide intermediates to form the oxo-radical-like intermediates (II); the activation of hydrocarbon molecules by these oxo-radical species in the *propagation* reactions (III); and finally, the *regeneration* of the Mn^{II} active sites via further oxidation of the alcohol to give aldehyde molecules (IV). For consistency of notation and ease of reference, here and in our future work examining this catalytic reaction, we retain the labeling of intermediates and reaction steps introduced in ref 25.

APPROACH AND METHODOLOGY

We have employed the AFI structure as representative of the class of nanoporous AlPO catalysts, first because of its simplicity: it comprises a one-dimensional noninterconnected 12-membered ring (MR) channel, with only one type of tetrahedral site in which to insert Mn; and second, since it is one of the systems that has been investigated most widely experimentally. In addition, the AFI structure can be easily prepared with a variety of organic templates and readily doped with a wide range of transition metals, including Co, Mn, and Fe, the most frequently used in aerobic catalytic oxidations.

It has long been recognized that divalent cations such as Mn^{2+} replace only Al^{3+} and not P^{5+} ions in tetrahedral positions within the aluminophosphate frameworks. Therefore, only one type of position is available for Mn in MnAPO-5 catalysts. The Mn-doped

AFI framework is described with periodic boundary conditions using the *P*1 space group (i.e., without any symmetry constraint), with the crystallographic unit cell (72 atoms): 1 Mn ion (replacing 1 Al) per AFI unit cell is inserted in a tetrahedral position. This doping level ensures no significant interaction between the Mn image sites because the distance between consecutive Mn ions is over 8 Å. The AFI unit cell dimensions are also large enough to prevent a strong interaction between the reactants in consecutive image cells. The initial unit cell parameters of the catalyst were obtained after full geometry optimization, including unit cell parameters, of the MnAPO-5 system, with Mn in the oxidized state, since this corresponds to the initial state of the catalyst in the absence of reactants; the unit cell parameters were then kept fixed for the rest of the calculations. This assumption is based on the fact that under reaction conditions (i.e. in the presence of the reactants), only a small number of active sites will interact with the reactant molecules, so the overall unit cell dimensions are dictated by the host catalyst itself and are unlikely to be modified. Moreover, no important energetic or structural differences are expected if the unit cell parameters are allowed to change during the study of the reaction pathways.

We have performed density functional theory calculations, as implemented in the program CRYSTAL,[26] using the hybrid-exchange functional B3LYP. The electronic distribution of the system is described as a linear combination of atomic orbitals, and the basis functions are expressed analytically as a contraction of Gaussian-type orbitals. A triple-valence plus polarization basis set for Mn and double-valence plus polarization for the other atoms, available from the online library of the CRYSTAL code,[27] have been employed. The excellent comparison between the predicted structure of the active sites in Fe-[28] and Mn-[4] AlPOs using this computational methodology and that obtained by X-ray absorption spectroscopy shows the reliable performance of the computational settings chosen. In addition, the same computational methodology was successfully applied to study the energetics of the decomposition of hydroperoxides in jet fuel autoxidation reactions,[29] an oxidation reaction similar to that studied here.

Preliminary calculations showed the high-spin state to be the ground electronic configuration both for Mn^{II} (d^5, with five unpaired electrons) and Mn^{III} (d^4, with four unpaired electrons), as expected owing to the low crystal field splitting caused by the π donor character of O-based ligands and the tetrahedral coordination of the transition metal ions in AlPO frameworks.

The AFI structure is composed of one-dimensional, non-interconnected 12-MR channels, whose walls are formed by 6-MR. These large channels are surrounded by smaller 6- and 4-MR channels, which are not large enough to permit the diffusion of the hydrocarbon reactants. Therefore, it is clear that the oxidation reactions will take place in the 12-MR channels, where the MnO_4 tetrahedra are part of the channel walls. In the case of Mn^{2+} (replacing Al^{3+}), the negative charge is compensated by the presence of a proton attached to one of the four nearest-neighbor O ions to Mn. Preliminary calculations showed that the most stable location for the proton is bonded to the O atom shared by the 12- and 4-MR channels, so we selected this position to study the initial H-transfer reaction.

To find the reaction pathway and locate reliably all stable intermediates and activation energies, the reactant species were moved in discrete steps (usually of 0.1 Å) along the reaction coordinate of each elementary reaction step. At each step, we performed constrained geometry optimizations, keeping the selected reaction coordinate frozen, but relaxing all other coordinates. This methodology allowed us to obtain the energy profile for each elementary step along the chosen reaction coordinate. The approximate transition state (TS) identified in this constrained search is very close to that obtained using second derivative-based methods, both in geometry (to within the step size chosen) and energy (usually less than 4 kJ/mol). Activation energies are calculated using the TS energy identified along the reaction profile, whereas fully optimized configurations for reactants and products were used to find reaction enthalpies for each elementary step. The oxidation state of the Mn active site in the different intermediates was identified by comparing the corresponding Mn atomic spin density with those of Mn^{III} (3.79 unpaired electrons) and Mn^{II} (4.83 unpaired electrons) in the AFI framework, all obtained with a Mulliken population analysis.

RESULTS

The main propagation cycle that leads to the production of the oxidative products (alcohol, aldehyde, and acid) requires the presence of active Mn sites in the reduced oxidation state (Mn^{II}) and of an initial concentration of hydroperoxide intermediate (CH_3CH_2OOH). Once these species are present, further hydroperoxide can be produced through the propagation cycle itself. However, in the initial reaction conditions, in which the MnAPO catalyst is calcined, all redox-active Mn sites are present in the oxidized (III) state. A preactivation step is required to transform the initial Mn^{III} sites into species that can enter the propagation cycle.

After an exhaustive set of calculations in which the interaction of each combination of reagent molecules with Mn sites has been explicitly examined, we propose the existence of a preactivation step, whose mechanism is summarized in Figure 1. The initial reaction conditions involve the presence of the hydrocarbon (RH) (hereafter, the CH_3CH_2 chain will be denoted as R), O_2, and the Mn site in its oxidized (III) state (**A**). We initially investigated whether any reaction could take place between Mn^{III} and O_2. Results showed that no $Mn^{III}\cdots O_2$ complex is formed: geometry optimizations always resulted in O_2 moving away from Mn, regardless of the O_2 spin and orientation, with Mn returning to its tetrahedral environment, due to the resistance of substitutional Mn^{III} in AlPO frameworks to any further oxidation. Once the $Mn^{III}-O_2$ interaction is ruled out, it becomes evident that the hydrocarbon molecules must intervene in the initial reaction step.

1. Formation of the Ethyl Radical (A → B). Our calculations show that the initial elementary step involves a hydrogen atom transfer from RH to the active site; the H atom bonds to the framework O nearest neighbor to Mn that is shared by 4- and 12-MR channels: the stable proton position in Me^{II}APO materials. The energy diagram for this reaction step, as well as the evolution of the spin on C and Mn and the C−H distance (corresponding to the dissociating bond), along the reaction coordinate are shown in Figure 2 (left). Here, the reaction coordinate is the distance between the dissociating H and the framework O atom forming the new O−H bond. The energy diagram shows an activation energy for this process of 135 kJ/mol and a reaction enthalpy of 93 kJ/mol. We can clearly observe that the C−H bond (blue line) remains stable as the hydrocarbon approaches the framework O (i.e., the active site) up to a (R)H−O(Mn) distance of 1.7 Å, where the bond starts to dissociate. The C−H bond dissociation and the consequent H-transfer to the framework

dx.doi.org/10.1021/cs100068t |*ACS Catal.* 2011, 1, 18–28

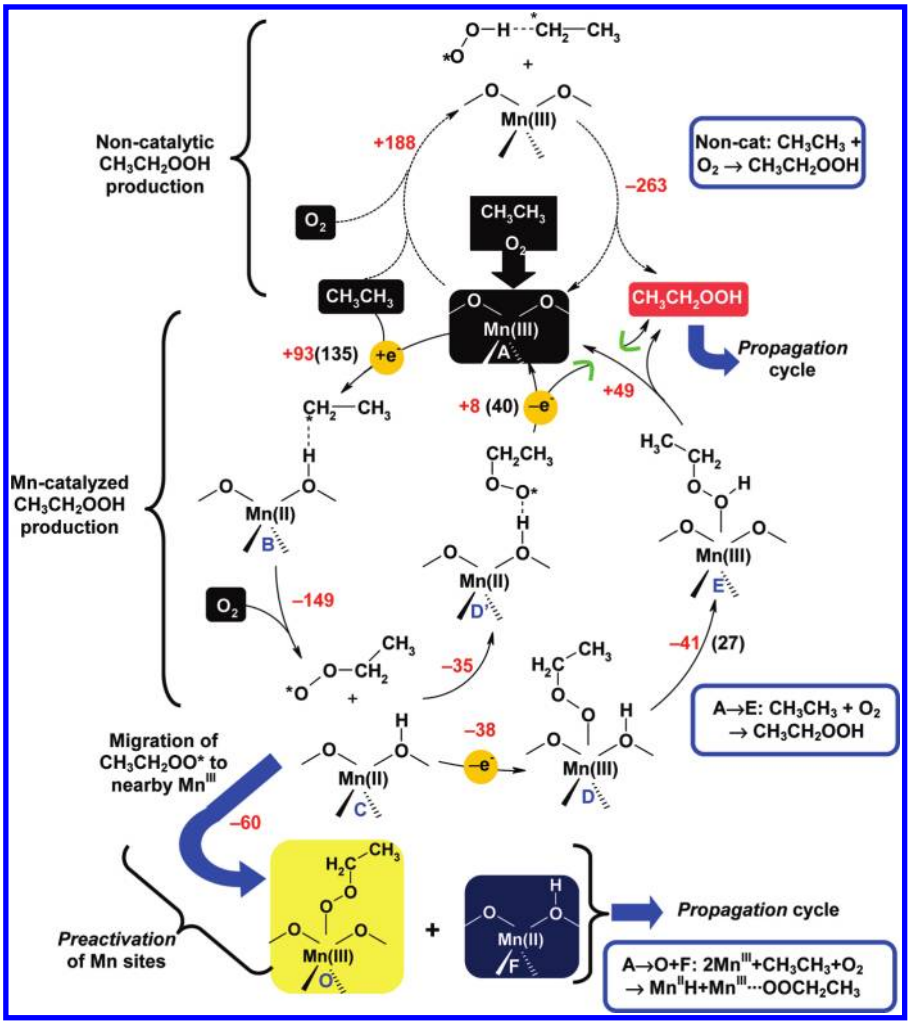

Figure 1. Preactivation mechanism (**A** → **E**) for the production of CH_3CH_2OOH from RH and O_2 without (top) and with the assistance of Mn^{III} (middle). A black background indicates initial catalyst and reactant molecules, and a red background highlights the hydroperoxide intermediate. Other background colors (yellow, blue) are used to indicate intermediates produced here that are necessary to initiate the subsequent propagation cycle. This cycle also yields activation of Mn sites through reduction of Mn^{III} to Mn^{II} (**F**, in blue background) and formation of the ROO···Mn^{III} complex (**O**, with yellow background) (**A** → **O** + **F**) after migration of ROO• radicals. Enthalpies (red) and activation energies, if any (black, in brackets), are shown for each elementary step, in kilojoules per mole.

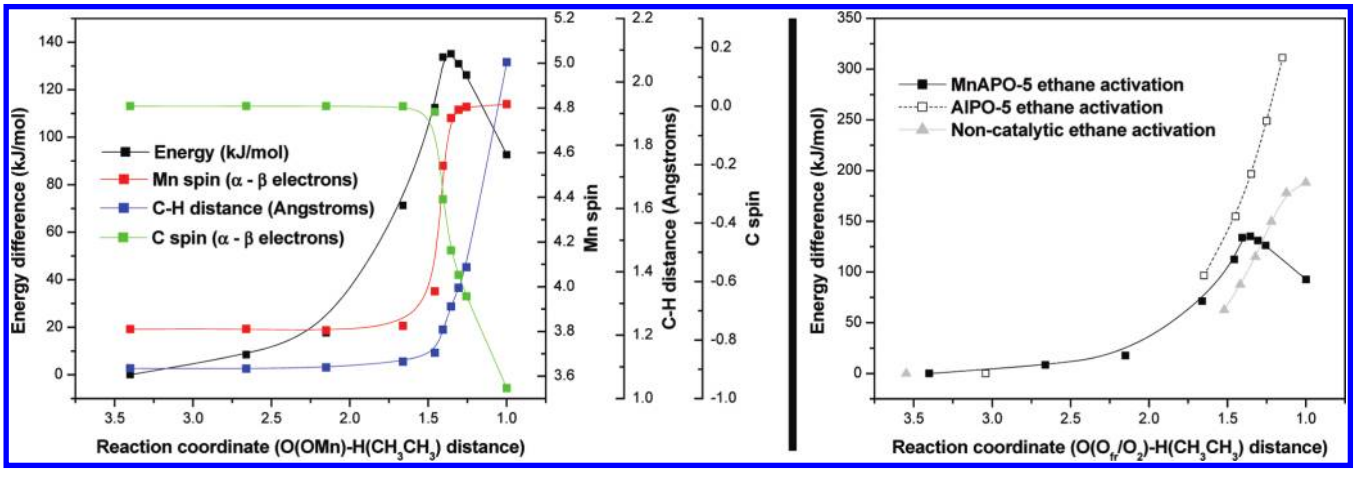

Figure 2. Left: Energy diagram (black line), evolution of Mn (red line) and of C (green line) spin, and of C−H distance (blue line) along the reaction coordinate (represented as the H(CH_3CH_3)−O(OMn) distance). Right: Energy diagram for the activation of ethane by MnAPO-5 (solid black line, solid squares), by undoped AlPO-5 (dashed black line, open squares) and by O_2 to give CH_3CH_2• and •OOH (solid gray line, square gray triangles).

dx.doi.org/10.1021/cs100068t |*ACS Catal.* 2011, 1, 18–28

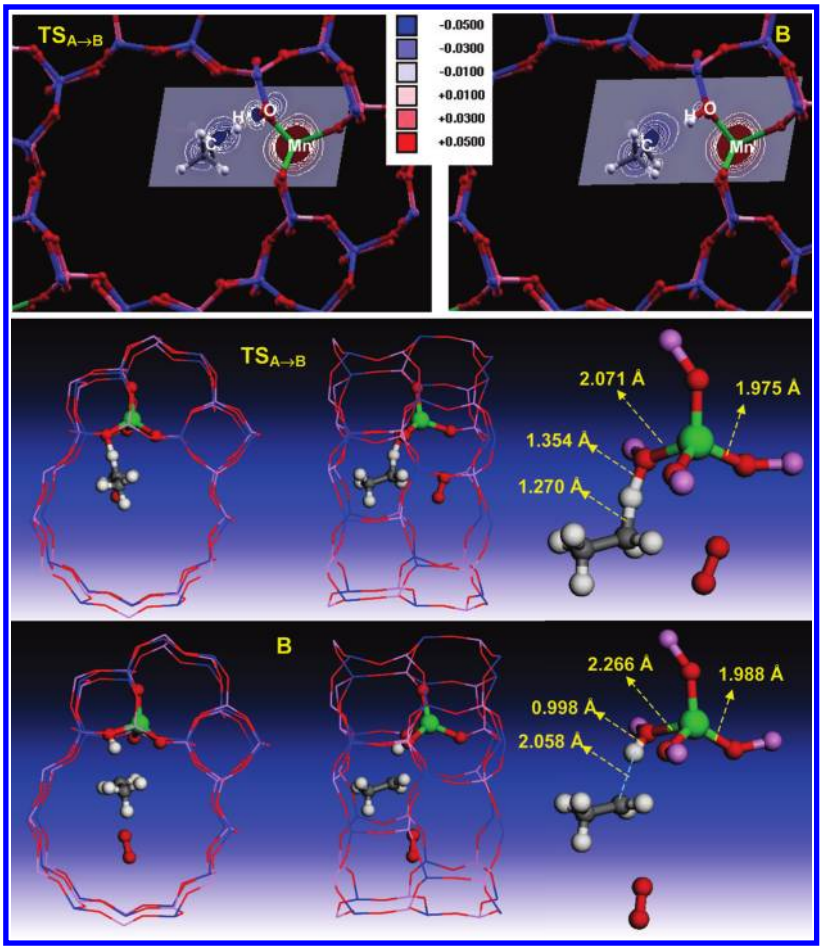

Figure 3. Top: Spin density maps of the transition state ($\mathbf{TS_{A\rightarrow B}}$) (left) and of the ethyl radical R• intermediate (**B**) (right); β and α spin densities are displayed in blue and red, respectively. White lines indicate isodensity lines. Middle: two views (left, middle) and detail (right) of the structure of the transition state ($\mathbf{TS_{A\rightarrow B}}$). Bottom: two views (left, middle) and detail (right) of the structure of the radical intermediate **B**.

results in a simultaneous increase in the Mn spin from 3.79 (corresponding to Mn^{III}) to 4.83 (corresponding to Mn^{II}), showing the reduction of Mn in this step (red line).

Mn is more stable in the II oxidation state (d^5), which has the maximum spin multiplicity (half-occupation of the Mn 3d electronic levels), thus providing the driving force for this initial step. The dissociation of the C−H bond leads to the formation of an ethyl radical (R•) (**B**), as shown by the evolution of the C spin from 0 to −1 (green line); that is, we have homolytic cleavage of the C−H bond, with the spin density being transferred to the C atom and the Mn site. The homolytic mechanism is also clear from the spin density maps of the transition state $\mathbf{TS_{A\rightarrow B}}$ (left) and the ethyl radical intermediate **B** produced in this elementary step (right), shown in Figure 3.

In the transition state, the β spin density (displayed in blue) from the C−H bond is shared between the C atom of RH (which is becoming a radical) and the framework O nearest-neighbor to Mn. The H atom has much smaller spin density: it mediates the radical transfer from C to the framework, but does not itself become spin-polarized. The electron associated with the homolytic dissociation of the molecular C−H bond is donated to the Mn^{III} site, whose spin density (red line in Figure 2 and red areas in Figure 3) increases upon approaching the TS. The completion of the H-transfer leading to formation of the Mn^{II}−R• intermediate (**B**) results in the β spin density being well-localized on one C of the ethyl radical, whereas the α spin density is taken up entirely by Mn, which is reduced to Mn^{II}. The H donated to the framework in this elementary step becomes a Brønsted acid proton, typical of a hydrogen atom neighboring low valent dopant ions (Mn^{II} in this case) in zeolites and AlPOs.

The molecular structure of the transition state ($\mathbf{TS_{A\rightarrow B}}$) and the radical intermediate (**B**) are also shown in Figure 3. In the transition state, the H atom is shared by the hydrocarbon and the active site, whereas after completion of the H-transfer, the CH_2 group of the ethyl radical becomes planar and is stabilized by strong interaction with the Brønsted acid site formed in the framework. The uptake of the hydrogen atom by the framework to form the intermediate **B** and the consequent Mn reduction cause, as expected, a substantial elongation of Mn−O bonds, in particular of that with the protonated oxygen.

All the calculations relating to this elementary step have been performed in the presence of one O_2 molecule in the AFI main channel, located next to the ethane molecule in the initial configuration. Our results suggest that O_2 does not intervene in this initial step and is always located far from the radical species upon geometry optimization at each step. We repeated all the calculations in the absence of O_2, and we obtained a very similar energy profile, with values of 134 and 92 kJ/mol for the activation energy and reaction enthalpy, respectively, demonstrating the lack of any direct involvement of O_2 in this step.

dx.doi.org/10.1021/cs100068t |*ACS Catal.* 2011, 1, 18–28

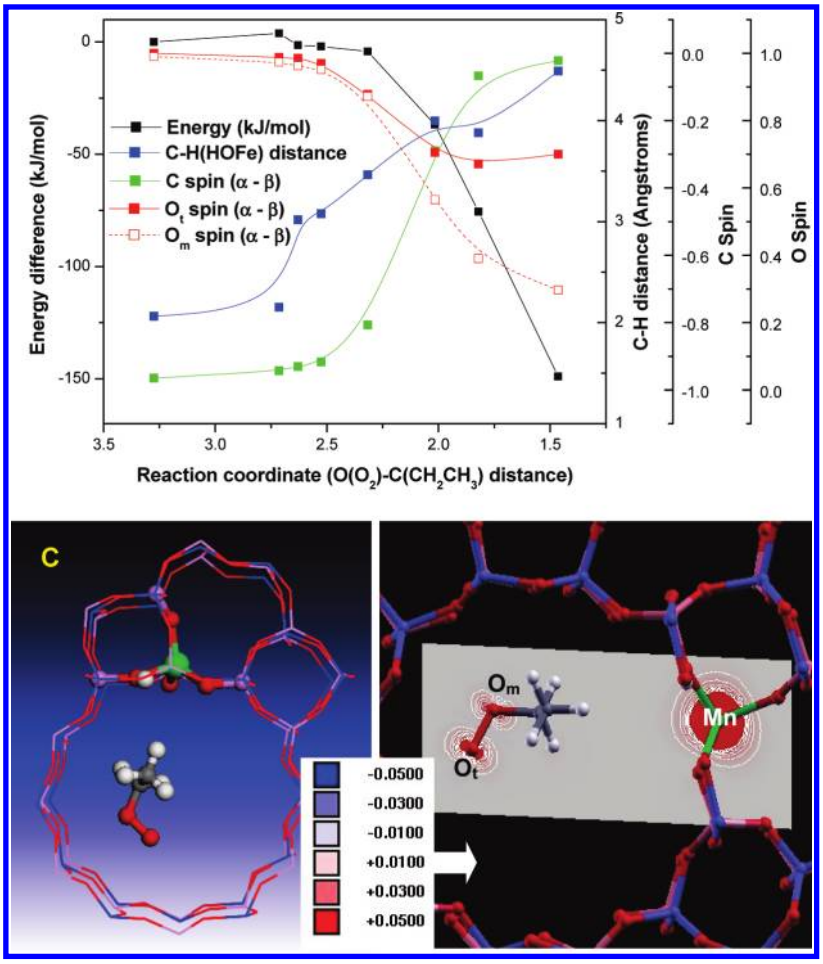

Figure 4. Top: Energy profile (black line), evolution of C (green line) and of O (red lines) spin, and evolution of C(CH_3CH_3)−H(HOMn) distances (blue line). Bottom: Molecular structure (left) and spin-density maps (right) of intermediate **C** (Mn^{II} + free CH_3CH_2OO• radical).

We further studied the influence of the Mn active site on this initial activation of ethane. To do so, we repeated the entire set of calculations inside an undoped AFI system, that is, with no Mn present in the framework. The energy profile corresponding to this system (empty squares in Figure 2, right) increases substantially upon elongation of the C−H bond and does not show any energy maximum corresponding to a TS, indicating beyond doubt that the presence of a redox-active site in the framework is essential for such a hydrocarbon activation. We also studied the activation of the hydrocarbon by O_2 without assistance of the Mn active site, that is, a noncatalytic pathway (Figure 1, top), but still occurring within the Mn-AFI channels. In this case, the H atom of the C−H dissociating bond is taken up by O_2, giving place to one ethyl (R•) and one hydroperoxo (•OOH) radical, species which are, indeed, stabilized by a strong interaction between the transferred H and the radical C in R•. Such an H-transfer reaction involves a reaction enthalpy of 188 kJ/mol, which is much higher than even the activation energies corresponding to the Mn-catalyzed ethane activation (135 kJ/mol). This noncatalytic activation mechanism will not therefore operate, showing again the essential role of Mn in the initial activation of the hydrocarbon molecules.

2. Addition of O_2 to the Ethyl Radical (B → C). Let us now discuss how the reaction cycle may progress after formation of the intermediate **B** ($Mn^{II}O(H)$−R•). Addition of O_2 to the ethyl radical can take place without significant activation barriers. It is therefore reasonable to expect that as soon as the R• radical (**B**) is formed, it is stabilized by attack of O_2 to the radical C atom. Due to the configuration of **B**, which interacts with the framework hydrogen, this attack can take place only from the opposite side of the CH_2 plane, since an attack from the top is sterically impeded by the presence of the channel wall, giving rise to an ethyl peroxo free radical (ROO•) that will be located in the middle of the channel (intermediate **C**). The energy profile and spin evolution of this process is represented in Figure 4. We observe that there is no (or only a very small) activation energy in this step, and indeed, it is a very exothermic process (−149 kJ/mol), leading to a substantial stabilization of the previously formed radical. The addition of O_2 involves a progressive separation of the R• radical from the framework proton, as shown by the evolution of the C(CH_3CH_2)-H(OMn) distance (blue line), leading to the disappearance of the interaction of the radical with the active site. In fact, the framework H is now oriented inside a 6-MR of the channel wall, and does not point to the channel. The spin evolution shows that the radical nature of the C atom is transferred to O_2 as it binds −the C spin varies from −1 to 0; the spin is then shared by the two molecular O atoms, which reduce their initial spin of 1 (in molecular O_2) to 0.7 and 0.3 −higher in the terminal O atom, as can be also observed in the spin-density map (Figure 4, bottom right).

It is of interest to understand if the two processes discussed so far, R• formation and subsequent O_2 addition to form the free

dx.doi.org/10.1021/cs100068t |*ACS Catal.* 2011, 1, 18–28

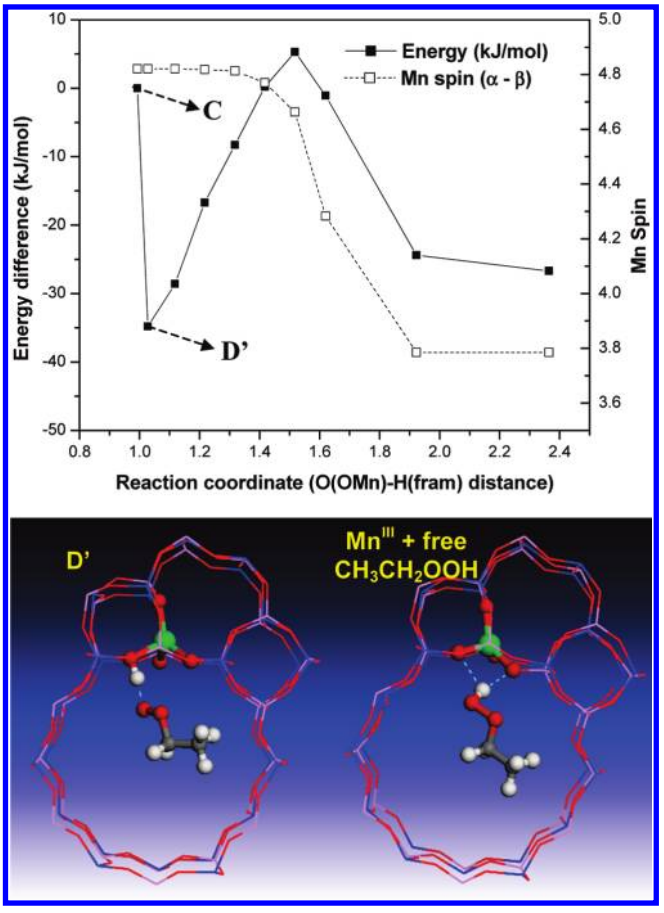

Figure 5. Energy profile (solid line, solid squares) and Mn spin evolution (dashed line, empty squares) (top) of the H-transfer reaction from the framework to the ROO• radical to form ROOH without complexation to Mn and structure of the reactant (left) and product (right) (bottom).

ROO•, could take place simultaneously in a concerted mechanism, avoiding the energy-demanding R• formation step. Our results suggest the opposite: they occur in subsequent elementary steps, going through the R• intermediate **B**, since a forced approach of O_2 to the nascent R• radical at any stage of the reaction coordinate resulted in O_2 moving away from R•, showing the need for the two subsequent steps and eliminating the concerted mechanism.

The free ROO• can undergo two different reaction pathways: an H-transfer reaction from the framework, leading to a hydroperoxide intermediate (3), or a migration along the AFI channel to a nearby Mn^{III} (4).

3. Formation of the Hydroperoxide (ROOH) Intermediate (C → A). To achieve the H-transfer reaction from the framework to form the hydroperoxide intermediate, the ROO• radical generated in the previous step needs to reorient within the AFI channel and approach the active site. Depending on the type of interaction with the active site, H-transfer can take place through two different mechanisms (3.A and 3.B).

3.A. ROO• can approach the active site in such a way as to form a strong H-bond with the framework proton (**D′**), which involves the framework H bending toward the center of the channel, as shown in Figure 5 (bottom left). This interaction stabilizes considerably the peroxo radical ($\Delta H = -35$ kJ/mol). From this intermediate, subsequent H-transfer to the peroxo radical can

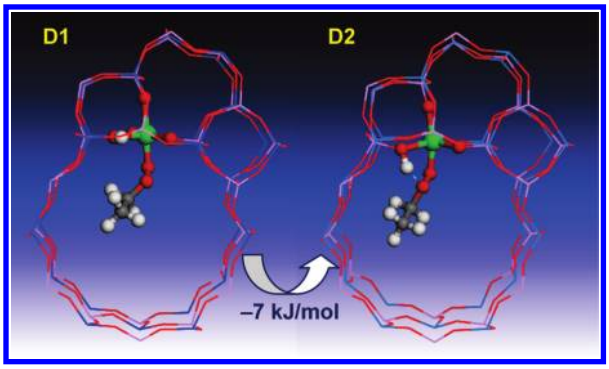

Figure 6. Molecular structure of the complexes (**D**) formed between ROO• and Mn^{II}.

easily take place, which leads to the formation of the hydroperoxide intermediate ROOH. The energy profile and spin evolution for such H-transfer is shown in Figure 5 (top); the step involves an activation energy of 40 kJ/mol, and a reaction enthalpy of +8 kJ/mol (from the adsorbed ROO• intermediate). To explain the slightly endothermic nature of this process, we note that although ROOH is a more stable species than the ROO• radical, its formation requires reoxidation of the Mn active site to Mn^{III}, the less stable oxidation state for Mn, as can be clearly seen from the Mn spin evolution in Figure 5 top, where the spin of Mn decreases from 4.82 (Mn^{II}) to 3.79 (Mn^{III}), with the transferred electron forming the new H−O bond. This pathway leaves ROOH and Mn^{III} sites free to undergo new reactions, thus closing the reaction cycle.

3.B. Alternatively, the free ROO• can approach the Mn^{II} active site and bind directly with Mn (**D1**) (Figure 6 left). In this mechanism, the free ROO• is stabilized by −31 kJ/mol. The interaction between two open-shell species (Mn^{II} and ROO•) leads to two spin multiplicities. The complex formed is more stable if the unpaired electron of the radical ROO• ligand has a spin opposite to that of Mn^{II} (for which $\Delta H = -31$ kJ/mol; the corresponding formation energy when Mn^{II} and ROO• have parallel spins is −25 kJ/mol). The spin of Mn in the complex (4.04), is between that of Mn^{II} (4.83) and Mn^{III} (3.79), but closer to Mn^{III}, which means that Mn has been partially oxidized upon formation of the complex; that is, an electron from Mn^{II} is used in the formation of a strong bond with the ROO• radical. The $Mn^{II}\cdots$ROO• complex can then be further stabilized (by −7 kJ/mol) by a rearrangement of the proton, which now stands out from the channel wall and orients toward the molecular O−O group, enabling the formation of an H-bond with the nonterminal molecular O atom (**D2**), resulting in the complete oxidation of Mn (spin of 3.86) to Mn^{III}. Such hydrogen orientation toward the radical ROO• provides the appropriate molecular structure for a subsequent H-transfer to the ligand to produce the hydroperoxide intermediate (ROOH) (**D** → **E**). The energy profile, atomic rearrangement, and Mn spin evolution for this H-transfer process, assisted by Mn, are shown in Figure 7 (top).

The approach of the proton to the terminal O atom, which is the distance selected as the reaction coordinate for this step, also causes a reduction of the distance between the proton and the nonterminal O atom (Om2-H distance displayed in red), with a simultaneous increase in the framework H−O distance, since the proton is now shared with the nonterminal molecular O (bottom left). Subsequently, the proton hops from the nonterminal to the

terminal O, a process that involves an activation energy of 27 kJ/mol, with the proton now closer to the framework O (solid blue line). The completion of this step involves a progressive transfer of the proton to the terminal O atom, which in turn involves a reoxidation of Mn^{II} to Mn^{III} and leads to the production of the hydroperoxide ROOH−Mn^{III} complex (**E**) (ΔH = −41 kJ/mol). Finally, this ROOH−Mn^{III} complex can dissociate and release ROOH and the reoxidized Mn^{III}, which is now free to undergo subsequent transformations, again closing the reaction cycle; this complex dissociation involves a relatively high energy (ΔH = +49 kJ/mol) owing to the high Lewis acidity of Mn^{III}.

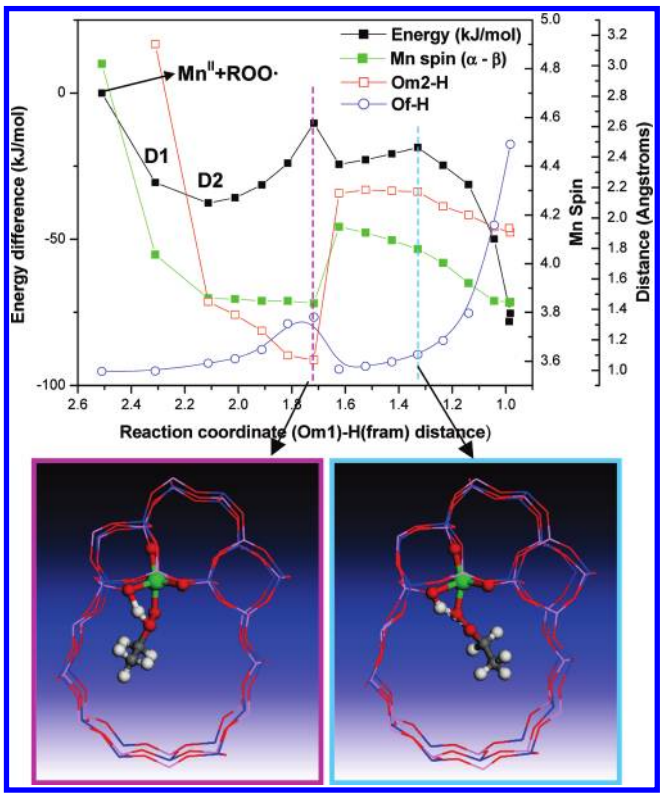

Figure 7. Energy profile, atomic rearrangement and spin evolution (top) of the H-transfer reaction from the framework to the ROO• ligand to form ROOH with the assistance of Mn. Bottom: molecular structure of TS intermediates at a reaction coordinate value of 1.7 (left, dashed pink line in top) and 1.3 (right, dashed cyan line in top), showing the hopping of the proton from the nonterminal to the terminal O.

The cycle described above leads to the production and accumulation of ROOH within the catalyst pores, in the presence of Mn^{III}, RH, and O_2. The net chemical transformation accomplished through steps **A** → **B** → **C** → **D** → **E** → **A** (or **A** → **B** → **C** → **D′** → **A**) is RH + O_2 → ROOH. As proposed previously (reaction 5 in the Introduction), ROOH could now be dissociated in the presence of Mn^{III} to produce chain-propagating intermediates. Hence, we investigated whether such a decomposition of ROOH can occur via the oxidized Mn^{III} site (Figure 8). ROOH forms a stable complex with Mn^{III} (**E**) (−49 kJ/mol), from which a H-transfer to the framework would lead to the ROO···Mn^{III} complex (**D**) (+41 kJ/mol). This pathway is the reverse of that previously discussed for the ROOH formation (Figure 1) (**A** → **E** → **D**); indeed, these steps could be avoided if the previous cycle ends at intermediate **D**, without evolving toward ROOH. An alternative propagation process from this intermediate can take place through H-transfer from a new RH molecule, resulting in the formation of ROOH and R•, the latter stabilized by interaction with ROOH (**V**). However, our results show that this step is very endothermic (ΔH = +99 kJ/mol) and thus unlikely to occur, as compared with the alternative ROOH formation (ΔH = −41 kJ/mol) described above. Such a highly endothermic initial step for the propagation cycle demonstrates that, although the subsequent addition of O_2 in R• is exothermic (−130 kJ/mol, **V** → **C**), propagation through Mn^{III} is unfavorable and will not occur, or at least it will occur to a much lower extent than through Mn^{II}. Moreover, even if this reaction may occur to some extent, it would just yield additional ROOH, showing that propagation from ROOH toward the oxidative products (alcohol, aldehyde, and acid) can take place only through Mn^{II}.

However, at this point, no reduced Mn^{II} is present in the catalyst as Mn^{II} sites in **C** are subsequently reoxidized in **D**, suggesting the need for an alternative reaction pathway to result in the net reduction of Mn^{III}.

4. Migration of ROO• to Nearby Mn^{III}. Let us go back to intermediate **C**: the ROO• radical when formed is located free in the middle of the channel, near a reduced Mn^{II}. The proximity of ROO• and Mn^{II} suggests their recombination into a ROO···Mn^{II} complex (**D**); however, due to the stereochemistry of the O_2 addition to R• (**B** → **C**), the radical points away from Mn and may therefore migrate away along the pores of the AFI structure, hence leaving behind a Mn^{II} in **C**. This process would generate the presence of Mn^{II} ions in the AFI channels, which would then be available for the dissociation of ROOH (**F**). The ROO• radical

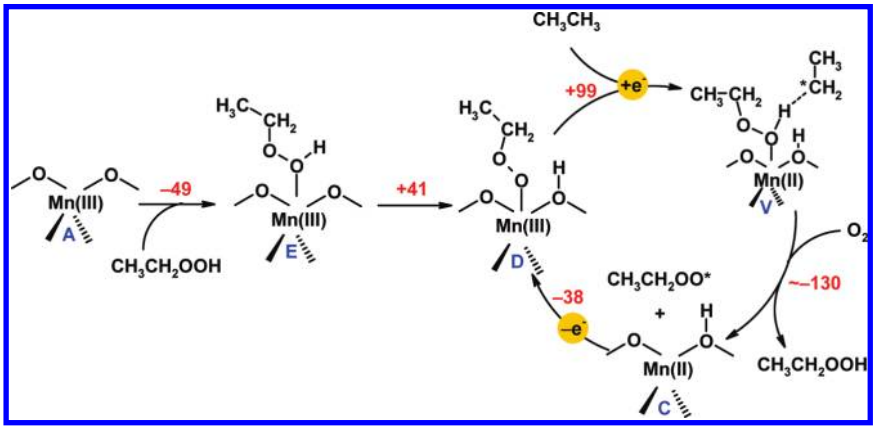

Figure 8. Propagation mechanism through Mn^{III}.

dx.doi.org/10.1021/cs100068t |*ACS Catal.* 2011, 1, 18–28

could instead approach another Mn^{III} site and form a new complex $Mn^{III}\cdots ROO\bullet$ (**O**). As before, both possible spin multiplicities were tried, and we found a higher stability when ROO• and Mn^{III} have opposite spins (the energy difference with the high spin complex is of 7 kJ/mol). The complex of ROO• with Mn^{III} is more favored than with Mn^{II} (**D**): the formation energies are −60 and −31 kJ/mol, respectively, due to the increased electron deficiency of Mn^{III}, which makes it a better acceptor for the electron donated by the peroxo radical. Overall, the migration of the ROO• radical away from the site where the original RH molecule has reacted yields not only the required Mn^{II} sites needed to activate the propagation reactions, but also $ROO\cdots Mn^{III}$ complexes (**O**) that can enter the propagation cycle, as shown in our earlier work.[25]

DISCUSSION

Our computational study provides a link between the initial reaction conditions, involving the presence of redox-active Mn^{III} sites, the hydrocarbon and O_2, and the species required for the transformation of the hydroperoxide intermediates into the final oxidative products (the alcohol, aldehyde, and acid) through the propagation cycle. As shown in our previous publication,[25] such a propagation cycle requires the presence of ROOH as well as reduced Mn^{II} sites, which can then be transformed through a series of reaction steps into $ROO\cdots Mn^{III}$ complexes (**O**), intermediates that can then lead to the production of new ROOH molecules. Either of these two species (i.e., Mn^{II} (with associated ROOH) or $ROO\cdots Mn^{III}$) could then initiate the propagation cycle, since they can be transformed into each other. Indeed, further ROOH molecules are produced through the propagation cycle, as was suggested by Iglesia and co-workers.[16]

Two different mechanisms for the activation of the hydrocarbon molecules can in principle be envisaged. The first is through a noncatalytic pathway, not involving the intervention of the Mn active site, where the C−H bonds are activated by O_2, leading to the production of R• and •OOH radicals. These two radicals can recombine to form ROOH, but alternatively, they could also evolve in the presence of O_2 toward the required Mn species for the subsequent propagation cycle: R• radicals could add O_2 to form ROO•, which could eventually bind a Mn^{III} site, yielding the $ROO\cdots Mn^{III}$ complex, whereas •OOH radicals could easily transfer the H atom to a framework O nearest-neighbor to Mn^{III}, promoting its reduction, a process that would be favored by the stability of reduced Mn^{II} sites. However, we showed that this noncatalytic activation of the hydrocarbon requires a high activation energy of 188 kJ/mol.

The most favorable hydrocarbon activation mechanism involves a reduction of the Mn active site through a H-transfer from the hydrocarbon to the nearest-neighbor O atom to Mn^{III}, which is reduced to Mn^{II}. Our results demonstrate that O_2 does not intervene at all in this activation process. The activation energy required for this H-transfer is 135 kJ/mol, which compares well with the experimentally observed value for the corresponding initial activation in the oxidation of cyclohexane by MnAPO-5 (155 ± 10 kJ/mol)[16] and is much lower than that for the noncatalytic pathway, showing the crucial role of Mn^{III} in the initial activation of the C−H bonds. The high activation energy of 135 kJ/mol also explains the long induction period observed experimentally in this type of oxidation reaction.

Once the R• radicals are formed, these are stabilized by addition of O_2 to produce ROO•. It is important to note that the addition of O_2 occurs via a stereospecific mechanism: since the R• radicals are not free inside the channels but stabilized by strong interactions with the framework proton (see Figure 2), one side of the C radical atom is blocked, and the O_2 attack will always take place from below the CH_2 plane. The reaction generates a free ROO• species with the terminal O atom not bonded to the active site but oriented to the center of the channel. Even if the R• radical is desorbed from the framework proton in **B** and locates free inside the channel, which has an energy cost of 16 kJ/mol, the product would still be a free ROO• radical.

This feature is crucial in our mechanism, since the nonbonded nature of the ROO• radicals allows two alternative pathways: one is a reorientation of ROO• so as to approach the original Mn^{II} active site, followed by recombination with the proton to form ROOH, which is indeed the first compound detected experimentally, and which causes the reoxidation of Mn. The second pathway involves a migration of ROO• along the channels away from the original Mn^{II} site, thus generating framework Mn^{II} sites that could initiate the propagation cycle. The ROO• radical can form a stable complex with another Mn^{III} site, favored by the stronger Lewis acid nature of Mn^{III} compared to Mn^{II}. The latter makes the migration of the ROO• radicals to other Mn^{III} sites a thermodynamically favored process (−60 kJ/mol for migration and complexation with Mn^{III} vs −38 kJ/mol for complexation with Mn^{II}), although the required migration of ROO• through the channel may have kinetic barriers.

In summary, this preactivation step can be described by the following chemical transformation: $RH + O_2 + 2Mn^{III} \rightarrow Mn^{II}(H^+) + Mn^{III}\cdots ROO\bullet$. Other than the effect on the reagent molecules RH and O_2, it transforms, with the assistance of one RH molecule and one O_2 molecule, two framework Mn^{III} sites, inactive in the propagation cycle, into one Mn^{II} site and one $Mn^{III}\cdots OOR$ complex, both active species in the propagation cycle. For this reason, we refer to this process as *preactivation*. This process is in line with the one suggested by Iglesia and co-workers in their model,[16] although in their mechanism, the ROO• radical was initially bonded to Mn, so it had to be first desorbed from the active site. Alternatively, the authors also suggested a migration of H species, rather than ROO• species, to nearby Mn sites as a preactivation mechanism, although we found this as a very unstable mechanism due to the instability of free radical H species. Interestingly, this process is required to occur just once for each pair of Mn sites, so only at the initial stages of the reaction. Once Mn^{II} and $Mn^{III}\cdots ROO\bullet$ sites are formed, they are regenerated in the propagation reactions of the catalytic process.

Once the preactivation has taken place, an alternative ROOH production mechanism becomes available: $Mn^{III}\cdots OOR$ (**O**) can yield ROOH through a propagation subcycle by means of H-transfer reactions from the RH hydrocarbon to the ROO• radicals, and subsequent O_2 addition to the R• that is formed.[25] Indeed, this route for ROOH production requires a much lower activation energy (E_a = ∼84 kJ/mol) than through preactivation (E_a = ∼135 kJ/mol) and, hence, will represent the main source of ROOH once Mn has been preactivated.

Let us now compare our computational results with the available experimental data. It is well documented that the addition of radical initiators such as *tert*-butyl hydroperoxide (^{t}BuOOH) reduces the induction period for aerobic oxidation.[8,10,16] This observation can be effectively explained by our model: ^{t}BuOOH is easily decomposed by Mn^{III} due to the

dx.doi.org/10.1021/cs100068t |*ACS Catal.* 2011, 1, 18–28

relative stability of ^{t}BuOO• radicals through H-transfer from ^{t}BuOOH to the active site (the calculated O−H bond energy in ^{t}BuOOH is 356 kJ/mol, much lower than the C−H bond energy in CH_3CH_3, 454 kJ/mol); indeed, for CH_3CH_2OOH (instead of ^{t}BuOOH), this O−H dissociation involves an activation energy of 68 kJ/mol and a reaction enthalpy of +41 kJ/mol, energies that are much lower than those in normal preactivation (135 and +93 kJ/mol, respectively). This ^{t}BuOOH dissociation would lead to the formation of Mn^{II} (with the proton attached to the framework O) and the corresponding peroxo-radical (^{t}BuOO•). In a similar way as for the CH_3CH_2OO• (ROO•) radical, this ^{t}BuOO• radical could migrate to a nearby Mn^{III} to generate Mn^{II} and the corresponding ^{t}BuOO···Mn^{III} complex (**O′**), which will then facilitate ROOH production through the propagation subcycle. This mechanism, which was previously suggested by Iglesia and co-workers,[16] avoids the initial energy-demanding direct activation of RH by Mn^{III}, providing an easier Mn preactivation mechanism, thus reducing the induction period.

Our model also provides an explanation for the lower reaction rate observed experimentally when the catalyst is initially in the reduced form:[16] Mn^{II} is efficient for dissociating ROOH, but cannot itself produce ROOH until it reaches the propagation subcycle, for which it requires the preliminary presence of ROOH. However, Mn^{II} itself cannot produce the initial ROOH, since it cannot be further reduced to abstract a hydrogen from the hydrocarbon: Mn^{II} would need to be first oxidized to Mn^{III} by O_2 and then carry out the preactivation. Alternatively, an initial formation of ROOH should take place through a noncatalytic mechanism, for instance, the direct reaction of RH and O_2 to form ROOH inside the catalyst pores. This reaction, however, as has been shown before, requires a higher activation energy (∼188 kJ/mol) than the catalytic preactivation through Mn^{III}. Hence, any of these alternatives would result in a decrease in the reaction rate, explaining the experimental observation.

In summary, our preactivation mechanism is in very good agreement with the scheme previously proposed experimentally by Iglesia and co-workers,[11,16] and indeed, our energy results support the hypotheses made there. However, the cycle proposed on the basis of the experimental evidence alone lacks much of the atomic level detail afforded by our computational study, thus showing the essential contribution that computational models can add to mechanistic experimental studies. The fact that the main lines of our computationally derived mechanism agree with ref 16 also validates our computational methodology, against one of the few reactions where such comparison can be made, thus giving confidence on the performance of current electronic structure methods in studying this kind of complex mechanistic problem.

SUMMARY AND CONCLUSIONS

Our computational work shows the important role that the so-called preactivation step plays in the initial stages of the aerobic oxidation of hydrocarbons catalyzed by Mn-doped nanoporous aluminophosphates. The initial reaction conditions involve Mn active sites in the (III) oxidation state. For the Mn sites to be active for the transformation of the hydrocarbons into the final oxidative products (alcohol, aldehyde/ketone, and acids), they must undergo a chemical transformation that involves a reduction to Mn^{II} and a parallel formation of alkyl peroxo radicals that will be stabilized by forming complexes with Mn^{III} (ROO···Mn^{III}). Both of these species are able to initiate the main propagation cycle.

Our results demonstrate the essential role of Mn in the initial activation of the hydrocarbon molecules: noncatalytic pathways, where the hydrocarbon molecules are activated by O_2 itself, require a much higher activation energy (∼188 kJ/mol) than the corresponding hydrocarbon activation by Mn^{III} (∼135 kJ/mol). Indeed, a system in which no Mn is present in the AlPO framework (AlPO-5) is not able to perform this type of hydrocarbon activation, showing the need for redox-active Mn ions to initiate the catalytic cycle.

To summarize, in this work, we have used state-of-the-art solid-state chemistry techniques based on hybrid exchange functionals in DFT and periodic boundary conditions to study successfully a complex heterogeneous catalytic reaction. Such a study has led to a detailed knowledge of the reaction mechanism, confirming and complementing the data available from experiments. Indeed, in such complex reactions, experiments alone cannot provide the full mechanistic picture, due to the short lifetime, instability, and complexity of the intermediates involved. Such a complete understanding of the catalytic mechanism is fundamental to design more efficient oxidation catalysts.

AUTHOR INFORMATION

Corresponding Author

*E-mails: (L.G.-H.) l.sainz@ucl.ac.uk, (F.C.) f.cora@ucl.ac.uk.

ACKNOWLEDGMENT

L.G.H. acknowledges funding from EPSRC (Grant EP/D504872). F.C. is supported by an RCUK Fellowship. We are grateful to Sir John Meurig Thomas, Gopinathan Sankar, and Claudio M. Zicovich-Wilson for helpful discussions. The authors acknowledge the use of the UCL Legion High Performance Computing Facility and associated support services in the completion of this work.

REFERENCES

(1) Wilson, S. T.; Lok, B. M.; Flanigen, E. M. U.S. Patent 4310440, 1982.
(2) http://www.iza-structure.org/databases/ (Accessed December 2, 2010).
(3) Saadoune, I.; Corà, F.; Alfredsson, M.; Catlow, C. R. A. *J. Phys. Chem. B* **2003,** *107,* 3012–3018.
(4) Corà, F.; Sankar, G.; Catlow, C. R. A.; Thomas, J. M. *Chem. Commun.* **2002,** 734–735.
(5) Thomas, J. M. *Angew. Chem., Int. Ed.* **1999,** *38,* 3589–3628.
(6) Arends, I. W. C. E.; Sheldon, R. A.; Wallau, M.; Schuchardt, U. *Angew. Chem., Int. Ed. Engl.* **1997,** *36,* 1144–1163.
(7) Hartmann, M.; Ernst, S. *Angew. Chem., Int. Ed.* **2000,** *39,* 888–890.
(8) Thomas, J. M.; Raja, R.; Sankar, G.; Bell, R. *Nature* **1999,** *298,* 227–230.
(9) Modén, B.; Oliviero, L.; Dakka, J.; Santiesteban, J. G.; Iglesia, E. *J. Phys. Chem. B* **2004,** *108,* 5552–5563.
(10) Thomas, J. M.; Raja, R.; Sankar, G.; Bell, R. *Acc. Chem. Res.* **2001,** *34,* 191–200.
(11) Modén, B.; Zhan, B.-Z.; Dakka, J.; Santiesteban, J. G.; Iglesia, E. *J. Phys. Chem. C* **2007,** *111,* 1402–1411.
(12) Raja, R.; Sankar, G.; Thomas, J. M. *Angew. Chem., Int. Ed.* **2000,** *39,* 2313–2316.
(13) Vanoppen, D. L.; De Vos, D. E.; Genet, M. J.; Rouxhet, P. G.; Jacobs, P. A. *Angew. Chem., Int. Ed. Engl.* **1995,** *34,* 560–563.
(14) Luna, F. J.; Ukawa, S. E.; Wallau, M.; Schuchardt, U. *J. Mol. Catal. A-Chem.* **1997,** *117,* 405–411.
(15) Raja, R.; Sankar, G.; Thomas, J. M. *J. Am. Chem. Soc.* **1999,** *121,* 11926–11927.

(16) Modén, B.; Zhan, B.-Z.; Dakka, J.; Santiesteban, J. G.; Iglesia, E. *J. Catal.* **2006,** *239*, 390–401.
(17) Concepción, P.; Corma, A.; López-Nieto, J. M.; Pérez-Pariente, J. *App. Catal., A* **1996,** *143*, 17–28.
(18) Zhou, L.; Xu, J.; Chen, C.; Wang, F.; Li, X. *J. Porous Mater.* **2008,** *15*, 7–12.
(19) Dugal, M.; Sankar, G.; Raja, R.; Thomas, J. M. *Angew. Chem., Int. Ed.* **2000,** *39*, 2310–2313.
(20) Raja, R.; Sankar, G.; Thomas, J. M. *Chem. Commun.* **1999,** 829–830.
(21) Raja, R.; Thomas, J. M.; Sankar, G. *Chem. Commun.* **1999,** 525–526.
(22) Sheldon, R. A.; Kochi, J. K. *Metal-Catalysed Oxidations of Organic Compounds*; Academic Press: New York, 1981.
(23) Hill, C. L. *Activation and Functionalisation of Alkanes*; John Wiley & Sons, Inc.: New York, 1989.
(24) Black, J. F. *J. Am. Chem. Soc.* **1978,** *100*, 527–535.
(25) Gómez-Hortigüela, L.; Corà, F.; Sankar, G.; Zicovich-Wilson, C. M.; Catlow, C. R. A. *Chem.—Eur. J.* **2010**, *16*, 13638−13645.
(26) Dovesi, R.; Saunders, V. R.; Roetti, C.; Orlando, R.; Zicovich-Wilson, C. M.; Pascale, F.; Civalleri, B.; Doll, K.; Harrison, N. M.; Bush, I. J.; D'Arco, Ph.; Llunell, M. CRYSTAL06; University of Torino" Torino, 2006.
(27) http://www.crystal.unito.it/Basis_Sets/Ptable.html (Accessed December 2, 2010).
(28) Zenonos, C.; Sankar, G.; Corà, F.; Lewis, D. W.; Pankhurst, Q. A.; Catlow, C. R. A.; Thomas, J. M. *Phys. Chem. Chem. Phys.* **2002,** *4*, 5421–5429.
(29) Zabarnick, S.; Phelps, D. K. *Energy Fuels* **2006,** *20*, 488–497.